

Identification of yield stress and plastic hardening parameters from a spherical indentation test

S. Kucharski*, Z. Mróz

Institute of Fundamental Technological Research, Surface Layer Laboratory, Swietokrzysja 21, 00-049 Warsaw, Poland

Received 7 August 2006; received in revised form 8 March 2007; accepted 18 March 2007

Available online 27 March 2007

Abstract

Assuming plastic hardening of metals are specified by the stress–strain curve in the form $\sigma = \sigma_0 + k\varepsilon_p^m$, the material parameters σ_0 , k and m are identified from spherical indentation tests by measuring compliance moduli in loading and unloading of the load–penetration curve. The curve $P(h_p)$ is analytically described by a two term expression, each with different exponents. Here, ε_p and h_p denote the plastic strain and permanent penetration. The proposed identification method is illustrated by specific examples including numerical and physical identification tests.

© 2007 Elsevier Ltd. All rights reserved.

Keywords: Spherical indentation test; Identification; Finite element modelling; Elasto-plastic material properties

1. Introduction and review of previous work

Conventional spherical indentation is one of the most convenient methods of identification of elastic moduli and plastic hardening parameters. The fundamental variables measured during the test are indentation force P , geometrical parameters such as contact radii a_t and a_p , penetration depths h_t and h_p determined in loaded and unloaded configurations, respectively, and the sphere diameter D . A review of extensive research related to identification methods based on indentation tests was presented in previous papers by the authors.

The fundamental solution of the spherical indentation problem for nonlinear elastic, rigid plastic and rigid viscoplastic materials was proposed in papers by Hill et al. [1], and Biwa and Storakers [2]. Attempts to make use of spherical indentation testing to identify material parameters has been considered in numerous papers. Let us mention Field and Swain [3], Adler and Dogan [4], Taljat et al. [5], Kucharski and Mróz [6,7]. In these papers, the authors try to eliminate the effect of elastic deformation on the measured indentation parameters and then make use of the “analytical” formulae given in papers [1,2].

The identification method proposed by Huber and Tsakmakis [8] is based on their numerical solution of the indentation problem. They have assumed constant moduli of isotropic and kinematic hardening, $E_t^{(is)}$, $E_t^{(kin)}$, and formulated the problem in dimensionless quantities. The two modes of hardening can be identified from the hysteresis loops that develop during the unloading–reloading test. In Refs. [9,10], these authors have proposed an identification procedure, which makes use of indentation test and neural networks methods. The global response data required in the identification procedure are load and penetration depth and the developed neural network method is applied in the cases of pure kinematic, pure isotropic, and mixed hardening.

An extensive numerical study of spherical indentation in an elasto-plastic half-space has been presented in the paper by Mesarovic and Fleck [11]. They considered the following modes of the indentation test: elastic (Hertzian) deformation, elastic–plastic, plastic self-similar, finite elastic deformation, and finite plastic deformation. The results of the elastic–plastic analyses are compared with rigid–plastic similarity solutions and the limits of validity of the similarity solution are investigated. Two elastic–plastic constitutive laws were considered:

$$\varepsilon = \frac{\varepsilon_0}{\sigma_0} \sigma \quad \text{for } \sigma \leq \sigma_0, \quad (1)$$

*Corresponding author. Tel.: +48 22 826 9806; fax: +48 22 826 9815.
E-mail address: skuchar@ippt.gov.pl (S. Kucharski).

$$\varepsilon = \left(\frac{\sigma}{K'}\right)^n \quad \text{for } \sigma > \sigma_o, \quad (2)$$

where

$$\frac{\sigma_o}{\varepsilon_o} = E, \quad \frac{1}{(K')^n} = \frac{1}{E} \left(\frac{1}{\sigma_o}\right)^{n-1} \quad (3)$$

and

$$\frac{\varepsilon}{\varepsilon_o} = \frac{\sigma}{\sigma_o} + \left(\frac{\sigma}{\sigma_o}\right)^n, \quad (4)$$

which corresponds to the familiar Ramberg–Osgood relation.

In Eq. (2), the total strain is expressed by a power law and in Eq. (4) only the plastic strain is expressed by this law. We note that the elasto-plastic constitutive laws (3) and (4) contain three independent parameters σ_o , $E = (\sigma_o/\varepsilon_o)$, n . The numerical simulations were performed for two values of n : $n \rightarrow \infty$ and $n = 3$. The following relations were calculated for different values of E/σ_o :

$$\frac{P_{av}}{(a/R)^{1/n}} \sim \frac{a}{R} \quad \text{or} \quad \frac{P_{av}}{(a/R)^{1/n}} \sim \frac{a}{R} \frac{E}{\sigma_o}, \quad (5)$$

$$c^2 \sim \frac{a}{R} \quad \text{or} \quad c^2 \sim \frac{a}{R} \frac{E}{\sigma_o}, \quad (6)$$

$$\frac{P}{\pi R^2 \sigma_o} \sim \frac{h}{R}. \quad (7)$$

These quantities were compared with the values of α , c^2 , and the function $P(h)$ resulting from the similarity solution. The role of friction and pre-existing stress within the half-space was also considered.

The authors conclude that the region of validity of the plastic similarity solution is limited by elastic effects for small contact loads and by finite deformation effects for large contact loads. Friction has a quantitative effect on the contact size only below the similarity regime, and in this regime the pre-existing stress has a minor effect on the indentation response. A result from the analysis is that the similarity solution cannot be used to identify material properties by means of simple indentation tests. The authors have also stated that extraction of material parameters may require more sophisticated indentation measurements than those currently practiced.

The procedure which enables the determination of the stress–strain curve using load–displacement curve measured in spherical indentation test has been presented in the series of papers by Nayebi et al. [12,13]. In their method, the following material model known as the Hollomon law is used:

$$\sigma = K\varepsilon^n = \sigma_y \left(\frac{\varepsilon}{\varepsilon_y}\right)^n, \quad \varepsilon_y = \frac{\sigma_y}{E}, \quad (8)$$

where ε is the elastic–plastic (total) strain, E denotes the Young's modulus, σ_y the yield stress, and n the strain hardening exponent. Here, the stress–total strain relation is

expressed in terms of a power law similar to Eq. (3). It is assumed in the identification procedure that the Young's modulus is known and only two parameters should be specified. By means of numerical simulations, the authors have determined the theoretical penetration curve, which represents the relationship between applied load P , indenter displacement h , σ_y , and n in the form

$$h = A(\sigma_y, n)P^{B(\sigma_y, n)}, \quad (9)$$

where

$$B = \frac{1}{(-0.151\sigma_y + 0.609)n + 0.09\sigma_y + 0.975},$$

$$A = [-3294 + 22170\sigma_y^{0.8}]e^{2.9n\sigma_y^{-0.323}}]^{-B}.$$

Let us note that relation (9) is not consistent from the point of view of dimensional homogeneity of right and left sides. The identification procedure is based on error minimisation between the experimental and theoretical penetration curves and leads to specification of σ_y and n . The identified curves were compared with those obtained from tensile tests for different steel types. The authors also proposed a method allowing for specification of the Vickers hardness from the identified parameters σ_y and n . For materials obeying the Hollomon law, a fair accuracy of identification was achieved. The authors suggest that for other materials one should introduce an appropriate law in their theoretical penetration curve model.

The same authors in Ref. [13] have generalized their approach to identify bimaterial systems. They proposed a law which accounts for the effect of both thin film and substrate on the penetration depth:

$$h^b = \alpha h^f + (1 - \alpha)h^s, \quad (10)$$

where $0 < \alpha < 1$, $\alpha = \alpha(\sigma_y^s, n^s, \sigma_y^f, n^f, e^f)$, e^f is the film thickness, and the subscripts b , f , and s correspond, respectively, to the bimaterial, film, and substrate. They discussed different formulae to calculate α which take into account specific plastic energies dissipated in the film and substrate. The formulae for approximation of dissipated plastic energy were also proposed and the proposed method enables the determination of $\sigma_y^s, n^s, \sigma_y^f, n^f$ for bimaterial systems, assuming that the Young's modulus is known. It was applied to determine mechanical parameters and Vickers hardness of samples with nitrided layers.

The method of determination of elasto-plastic properties by sharp indentation tests has been proposed in the paper by Giannakopoulos and Suresh [14]. They presented a general theoretical framework for instrumented sharp indentation and outlined their identification method.

The identification of material parameters by means of sharp indentation testing has also been proposed in the paper by Tunvisut et al. [15]. They have considered a three-parameters material model (8) and proposed the following formulas, which relate material constants and indentation

parameters:

$$\frac{P_m}{Eh_m^2} = 73\varepsilon_y^{0.82} - 87.3\varepsilon_y^{0.98} - (0.24 \ln \varepsilon_y + 0.36)n^{0.26 \ln \varepsilon_y + 0.10}, \quad (11)$$

$$\frac{A_f}{h_m^2} = 6 \ln \varepsilon_y - 178\varepsilon_y^{0.13} + (4.54 \ln \varepsilon_y + 5.86)n^{0.1 \ln \varepsilon_y - 0.10} + 155.7, \quad (12)$$

where P_m and h_m are the maximum indentation load and depth, respectively, A_f is the indentation area after unloading, where $\varepsilon_y = \sigma_y/E$ is the elastic strain limit. The authors have compared tensile stress–strain curves for steel specified by the proposed method and obtained in tensile tests. They have also identified properties of Mo and AlSi coatings.

To correlate plastic properties of materials with hardness defined as a ratio of applied load to the projected area of the indentation, the so-called expanding cavity models were developed. For elastic–perfectly plastic materials, this model was proposed by Johnson [16]. Recently, the model was enhanced for spherical and conical indentation of elastic power-law hardening and elastic linear-hardening materials by Gao et al. [17]. Their approach is based on elastic–plastic solutions for internally pressurized thick-wall spherical shells. They have derived relations between H/σ_y , E/σ_y , and strain hardening exponent n . Parametric study of the developed model was conducted; however, a procedure for identification of material parameters has not been proposed.

The identification method based on notion of representative strain defined for spherical indentation was proposed by Cao et al. [18]. The Hollomon law, (8), was used as a material model. To specify σ_y and n , the indentation test should be performed at two different penetration depths and the reduced Young modulus E^* should be known. The authors have emphasized that if h/R is too small, a deformation is dominated by elasticity and identification is not possible. The values of h/R assumed in the identification procedure are $h/R = 0.01$ and $h/R = 0.06$. The method was verified using the parameters of four typical metals, $132 \leq E/\sigma_y \leq 600$, $0.1 \leq n \leq 0.25$.

The present work constitutes an extension to and improvement upon the previous identification method discussed in detail by Kucharski and Mróz [19], where the compliance moduli of the load–penetration curve were used in order to specify plastic hardening parameters. The identification procedure is based on the proposed analytical expression of indentation force–permanent penetration depth dependent on a set of material parameters. It is believed that this expression is more reliable than the assumed *ad hoc* empirical expressions, such as those presented by Eqs. (9) or (11), as it results from the analytical similarity solution. The permanent penetration depth and its relation to indentation force was specified by carrying out consecutive unloading–reloading programs

during the spherical indentation test. The details of the procedure were described in previous papers [7,19].

2. Proposed relation of load–permanent penetration

We assume the small strain theory and decompose the total strain ε into elastic and plastic portions, $\varepsilon = \varepsilon_e + \varepsilon_p$. When a rigid–plastic material model is considered, the elastic strain is neglected, $\varepsilon_e = 0$, and the plastic strain can be expressed as a function of stress. When the power hardening rule is used, then the stress–strain curve in uniaxial tension can be described by the relation

$$\varepsilon_p = \left(\frac{\sigma}{k}\right)^{1/m} \quad \text{or} \quad \sigma = k\varepsilon_p^m \quad (13)$$

where σ denotes the Cauchy stress and m, k are the material parameters. For this type of homogeneous relation, a self-similar solution can be generated and the relation force–penetration depth, for $0 < m < 1$ denoted as $P_m(h_p)$, is expressed in the form, cf. Biwa and Storakers [2]

$$P_m = \pi\alpha k\beta^m [c(m)]^{2+m} D^2 \left(\frac{h_p}{D}\right)^{(m/2)+1}, \quad (14)$$

where $\alpha = 3.07$, $\beta = 0.32$ are constants, D the sphere diameter, and the parameter c is defined as

$$c^2 \equiv \frac{a^2}{h_p D} \quad (15)$$

(a is radius of contact) and depends only on the hardening exponent m according to the formula

$$c^2(m) = 1.41 \exp(-0.97m). \quad (16)$$

Introducing notation $c(m \neq 0) = c_h$ we can rewrite (14) as follows:

$$P_m = \pi\alpha k\beta^m c_h^{2+m} D^2 \left(\frac{h_p}{D}\right)^{(m/2)+1}.$$

In particular, when $m = 0$, a perfectly plastic response is predicted from Eq. (13) with k identified as the yield stress $\sigma = k = \sigma_0$

and the relation force–penetration depth, here denoted as $P_0(h_p)$, has a form

$$P_0 = \pi\alpha\sigma_0 c_0^2 D^2 \frac{h_p}{D}, \quad (18)$$

where $c_0 = c(0)$, $c_0^2 = 1.41$, and a linear dependence of force on h_p occurs. It should be noted that in the case of rigid–plastic material law (13), the self-similar solution (14), (18) results from exhaustive dimensionless analysis presented in Refs. [1,2] and can be considered as an “exact” analytical solution of the indentation problem.

A more complex case occurs when the plastic strain develops after exceeding the yield stress, so that

$$\varepsilon_p = \left(\frac{\sigma - \sigma_0}{k}\right)^{1/m} \quad \text{for } \sigma > \sigma_0 \quad \text{and} \quad \varepsilon_p = 0 \quad \text{for } \sigma < \sigma_0, \quad (19)$$

and the familiar Ludwig relation is obtained

$$\sigma = \sigma_0 + k\varepsilon_p^m \tag{20}$$

The self similar solution (14) does not occur in this case. However, as the material stress–strain relation (20) is a superposition of laws (13) and (17), we postulate that the relation $P-h_p$, which in this case is denoted as $P_T(h_p)$, can be expressed as a weighted superposition of solutions (14) and (18) which in turn correspond to two terms of the stress–strain relation (20), thus

$$P_T(h_p) = w_1 P_o(h_p) + w_2 P_m(h_p), \tag{21}$$

where w_1, w_2 are coefficients which should be determined. Let us analyze the characteristic response curves obtained for self-similar solutions (14) and (18) for $0 < m < 1$ and $m = 0$ presented in Fig. 1a,b. Following this analysis we can confirm the form of Eq. (21) and specify the coefficients w_1 and w_2 . It is seen that c^2 does not depend on P and is a function of m , $c^2 = c^2(m)$, reaching the maximal value for $m = 0$ and decreasing with m . The contact compliance dh_p/dP is constant for $m = 0$ but for

$m > 0$, when $P \approx 0$ then dh_p/dP tends to infinity and then decreases with growing P .

When the non-homogeneous material stress–strain relation (20) is used, we postulate that these curves should have the form shown in Fig. 2. In fact, as (20) can be approximated by (17) and (13) respectively for $\varepsilon_p \rightarrow 0$ and for increasing values of ε_p , we assume that the form of curve $P_T(h_p)$ is similar to (18) for small penetration depths (i.e. $P_m/P_o \rightarrow 0$ when $h_p \rightarrow 0$) and can be approximated by (14) for large penetration depths. Consequently, the contact compliance will decrease from its initial finite value $1/T$, Fig. 2, corresponding to a perfectly plastic response, where T cf. (29) depends uniquely on initial yield stress σ_0 and does not depend on hardening parameters (oppositely to similarity solution where the initial compliance tends to infinity for $m > 0$). This assumption is close to the conclusion made by Gao et al. [17] and Park and Pharr [20]. In fact they have observed that for the Hollomon law, the value of hardness does not depend on strain hardening exponent for small penetration depths.

In particular, c^2 now depends on P , $c^2 = c^2(P, m, k, \sigma_0)$, and decreases from its initial value $c_0^2 = 1.41$. This initial value (for $P \rightarrow 0$) does not depend on material parameters in the law (20) and corresponds to the similarity solution for $m = 0$. The assumption on the variation of c^2 was confirmed in numerical experiments presented in the next section, where the cyclic loading–unloading–reloading curves were determined by means of FEM for all materials presented in Table 1. Next, the curves $h_p(P)$ were generated using a segment subtraction method described in Ref. [7], and the values c according to definition (15) were calculated from

$$c^2(P_i) = \frac{a^2(P_i)}{Dh_p(P_i)} \tag{22}$$

for different values of force reversals P_i . Alternatively, the function $h_p(P)$ can be calculated by integrating the plastic compliance curve dh_p/dP . The diagram $c^2(P)$ for materials II and IV, cf. Table 1, is presented in Fig. 3 where one can

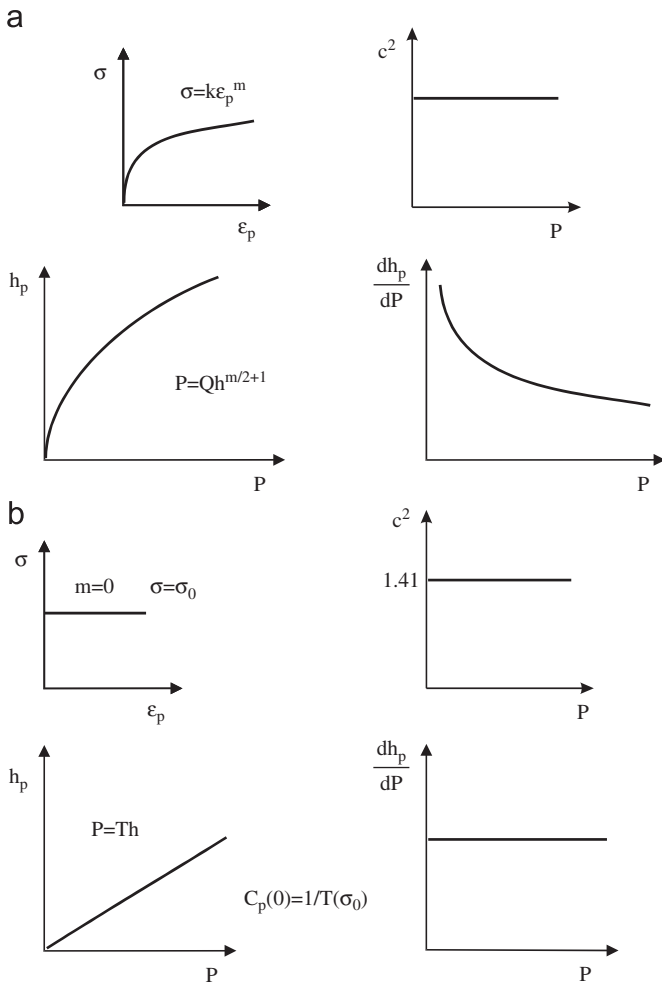


Fig. 1. Characteristic response curves for the similarity solution: (a) plastically hardening material, $0 < m < 1$; (b) perfectly plastic material, $m = 0$.

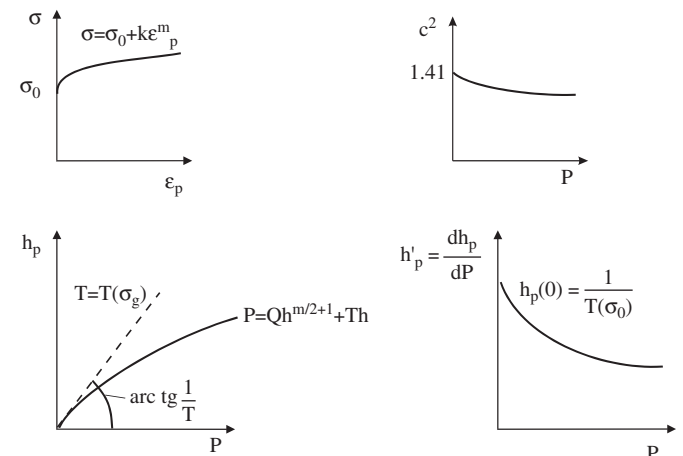


Fig. 2. Characteristic response curves for the proposed weighted superposition solution.

Table 1
Parameters of plastic stress–strain curves for considered materials

	Number of σ – ε_p curve					
	I	II	III	IV	V	VI
Stress–plastic strain relation	$\sigma = 290 + 610\varepsilon_p^{0.56}$ (MPa)	$\sigma = 290 + 1350\varepsilon_p^{0.65}$ (MPa)	$\sigma = 490 + 610\varepsilon_p^{0.56}$ (MPa)	$\sigma = 490 + 1650\varepsilon_p^{0.7}$ (MPa)	$\sigma = 290$ (MPa)	$\sigma = 490$ (MPa)

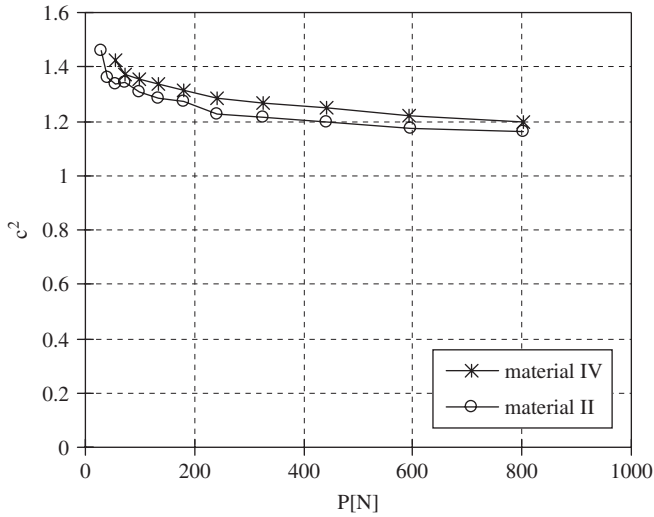


Fig. 3. Variation of c^2 for materials obeying Ludwig law.

observe that $c^2(P)$ decreases. Its variation is greater for low loading ranges than for larger values of loading (large deformation), where it is close to a constant value. This results from the fact that for large deformations, the Ludwig tension curve (20) can be approximated by a power curve for which the similarity solution is valid and c^2 does not depend on P , cf. Eq. (16). Generally, in the case of material law (20), for small loading the response curves are close to those obtained from the similarity solution for $m = 0$; in the range of large indentation forces, the response curves corresponding to Eq. (20) are close to those obtained from the similarity solution for $m > 0$.

Consider now an indentation test of three materials: an actual material described by the Ludwig law (20), a material denoted as M_o which fulfils power law (13) for $m = 0$, and a material denoted as M_h , which fulfils power law (13) for $m > 0$. Materials M_o and M_h can be considered as fictitious components of the actual material characterized by the law (20). Let us note that $a^2 = c^2 h_p D$, so for the same penetration depth $h_p = h_{pa}$ the contact areas F_o , F_h , F_a for material M_o ($m = 0$), material M_h ($0 < m < 1$) and the actual material are different, thus we have

$$\frac{F_a}{F_o} = \frac{a_a^2}{a_o^2} = \frac{c_a^2}{c_o^2}, \quad \frac{F_a}{F_h} = \frac{a_a^2}{a_h^2} = \frac{c_a^2}{c_h^2}, \quad a_h < a_a < a_o, \quad c_h < c_a < c_o, \quad (23)$$

where a_a and c_a^2 correspond to the tested actual material (20), a_o and $c_o^2 = c^2(m = 0) = 1.41$ —to the material M_o ,

and a_h , $c_h^2 = c^2(m \neq 0)$ correspond to the material M_h , cf. Fig. 4. Note, that both values c_o^2 and c_h^2 can be determined from formula (16) resulting from the similarity solution and c_a^2 should be determined from Eq. (15) or (22) (the subscripts a , o , h correspond to materials: actual, M_o and M_h , respectively). Assuming that the actual material is a compound of M_o and M_h and taking into account different contact areas produced in the indentation of each component, we postulate that the mean pressure which appears in the indentation test of the compound material is a simple sum of mean pressures developed by indentation of each component at the same penetration depth $h_p = h_{pa}$:

$$\frac{P_T(h_p)}{a_a^2} = \frac{P_o(h_p)}{a_o^2} + \frac{P_m(h_p)}{a_h^2}. \quad (24)$$

In view of (23), we can now determine the correcting weight factors w_1 and w_2 in Eq. (21) accounting for different contact areas, thus

$$\begin{aligned} P_T(h_p) &= \frac{c_a^2}{c_o^2} P_o(h_p) + \frac{c_a^2}{c_h^2} P_m(h_p) \\ &= \pi \alpha D^2 \left[\sigma_o c_a^2 \frac{h_p^2}{D} + k c_a^2 \beta^m c_h^m \left(\frac{h_p}{D} \right)^{1+m/2} \right]. \end{aligned} \quad (25)$$

Let us introduce the transformed load

$$Z_T(h_p) = \frac{P_T(h_p)}{c_a^2(P_T)} = \pi \alpha D^2 \left[\sigma_o \frac{h_p}{D} + k \beta^m c_h^m \left(\frac{h_p}{D} \right)^{1+m/2} \right], \quad (26)$$

where $c_a^2 = c_a^2(h_p)$ or $c_a^2 = c_a^2(P)$, is a decreasing function of h_p or P . The $c_a(P_T)$ curves were determined from numerical experiments using (22) for all identified materials (Table 1), and the results for materials II and IV are presented in Fig. 3. Taking into account a form of experimental $c_a(P_T)$ curves in Fig. 3, we can describe them using the following function:

$$c_a^2(P) = (c_h^2 - c_o^2)(1 - e^{-\eta P}) + c_o^2, \quad (27)$$

where c_o is the initial value, c_h is the asymptotic value corresponding to large P , and η denotes a parameter of actual material. Note, that $c_o = 1.41$, c_h is the unique function of m specified by (16), and the constant η can easily be determined using curve fitting procedure when the points $c_a(P_i)$ are known. Eqs. (26) and (27) will constitute the foundation for the identification procedure; however this procedure requires the function $c_a(P_T)$ to be specified only at some discrete set of points P_i .

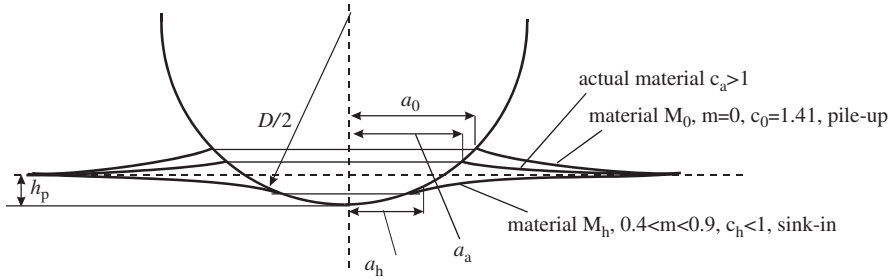


Fig. 4. Contact geometries for materials I and II and the actual material.

3. Identification of material parameters

Formula (26) can be presented in a simplified and modified form

$$Z_T \left(\frac{h_p}{D} \right) = T(\sigma_o) \frac{h_p}{D} + Q(m, k) \left(\frac{h_p}{D} \right)^{1+m/2+w}, \quad (28)$$

where

$$T(\sigma_o) = \pi \alpha D^2 \sigma_o, \quad Q(m, k) = \pi \alpha D^2 k \beta_1^m c_h^m, \quad (29)$$

and the exponent in the second term of (28) was assumed as $1 + m/2 + w$ instead of $1 + m/2$, where w may constitute a correction factor used to improve the accuracy of prediction. For the same reason in Eq. (29) the parameter β is replaced by β_1 . The constants β_1 and w should be calibrated by means of numerical simulations of indentation tests for numerous sets of material parameters.

The identification procedure is composed of the following steps:

1. Measurement of the cyclic loading–unloading–reloading penetration curve with load reversals at $P = P_i$; determination of points $dh_p/dP(P_i)$ of the plastic compliance curve $C^p(P)$, cf. Ref. [19], and of the plastic penetration curve, $h_p(P_i)$, calculated as an integral of the compliance curve

$$h_p(P_i) = \int_0^{P_i} C^p(P) dP.$$

2. Measurement of contact radius a for values of P_i corresponding to load reversals; calculation of $c_a^2(P_i)$ specified by (22) and $Z_i(h_{pi}/D) = P_i(h_{pi}/D)/c_a^2(P_i)$ according to (26).
3. Specification of T and then σ_o using the intersection point of the plastic compliance curve with the ordinate axis

$$\sigma_o = \frac{T}{c^2(0)\pi\alpha D^2} = \frac{1}{C^p(P \approx 0)} \frac{1}{1.41\pi\alpha D^2}. \quad (30)$$

4. Specification of k and m based on the condition of the best fit of function

$$s = Q(m, k) \left(\frac{h_p}{D} \right)^{1+m/2+w}, \quad (31)$$

to the points

$$\left(\frac{h_{pi}}{D}, Z_i' \right),$$

where

$$Z_i' = Z_i - T \frac{h_{pi}}{D}.$$

It should be mentioned that the approximate formulae (25–29) and identification Eqs. (30,31) correspond to the rigid–plastic material (20). As it is seen from identification procedure, the following functions should be specified:

- (1)

$$\frac{dh_p}{dP}(P)$$

- (2) $a(P)$ and $h_p(P)$ which in turn are used to calculate $c_a^2(P)$.

The identification procedure can be applied to identify both rigid plastic and elastic–plastic material. In the case of rigid–plastic material, the functions $h_p(P)$, $a(P)$ can be specified directly from the experiment consisting of monotonic loading, and then from the specified function $h_p = h_p(P)$ one can calculate dh_p/dP by simple differentiation. The accuracy of the determination of these functions does not depend on the material parameters.

In the case of an elastic–plastic material, the function $a = a(P)$ can also be specified directly from measurement, provided it is assumed that a has the same value in loaded and unloaded configurations. It follows from this assumption that a can be measured in the unloaded configuration with indenter removed from residual imprint, as a half of diameter of boundary of the imprint. This assumption was discussed in our previous work [6], and was accepted by other researchers. It is justified if the ratio E/σ_o is maintained in a range common for metals and a/D is in a range for which the similarity solution is valid and it enables to specify a with a sufficient accuracy. The remaining functions, $h_p = h_p(P)$ and $dh_p/dP = h_p'(P)$ should be evaluated from the cyclic elastic–plastic penetration curve. This evaluation is composed also of two steps but their order is different than in the case of a rigid–plastic material. First the values of function $h_p'(P)$ in discrete

points P_i should be extracted from the cyclic loading–unloading–reloading penetration curve using elastic–plastic and elastic compliance subtraction at the load reversal points P_i , cf. Ref. [19],

$$\frac{dh_p}{dP}(P_i) = \frac{dh_{ep}}{dP}(P_i) - \frac{dh_e}{dP}(P_i). \quad (32)$$

Next the $h_p(P)$ function is calculated by means of integration. These curves correspond to a certain fictitious rigid plastic material which fulfils the law (20), and the strain hardening parameters σ_o , n , k of this material are the same as for the tested actual elastic–plastic material.

The accuracy of determination of the compliance modulus $h'_p(P_i)$ depends on material parameters, namely on the ratio E/σ_o . Thus, for the elastic–plastic material, the evaluation of $h_p(P)$ and dh_p/dP should be performed very carefully as its accuracy affects the accuracy of the whole identification process. The advantage of the method lies in the fact that the accuracy of determination of $h'_p(P)$, and consequently the accuracy of identification of plastic hardening parameters, is not affected by an experimental frame compliance; that is, the effect of elastic compliance is automatically removed when Eq. (32) is applied. The elastic and plastic parameters of the stress–strain curve are now specified independently. These observations are illustrated in the examples presented below.

4. Application of the proposed identification method: numerical experiments

To verify the proposed method for the case of elastic–plastic materials, several numerical experiments have been performed. Numerical simulation of cyclic indentation tests was performed for materials labeled as I, II, III, IV, V, VI for which the material parameters σ_o , k , and m were assumed as presented in Table 1. These parameters were then determined by applying the proposed identification procedure.

As observed, materials I and II are characterized by the same initial yield stress $\sigma_o = 290$ MPa and different hardening exponents. Similarly, materials III and IV have the same yield stress and differing hardening parameters. Materials V and VI are introduced to illustrate specific cases of the identification procedure for the elastic–perfectly plastic response with yield stress values the same as for materials I, II and III, IV respectively. The respective curves σ – ε_p , for six materials are shown in Fig. 5. To illustrate the range of applicability of the proposed method and its sensitivity on the material parameters, different ratios E/σ_o are considered.

The numerical indentation experiments were performed using MARC[®] finite element code. The finite element mesh of the indented half-space was composed of 5666 elements and 5817 nodes. The spherical indenter of diameter $D = 2.5$ mm was modeled as a rigid body. The details of the finite element mesh have been discussed in the previous paper [6].

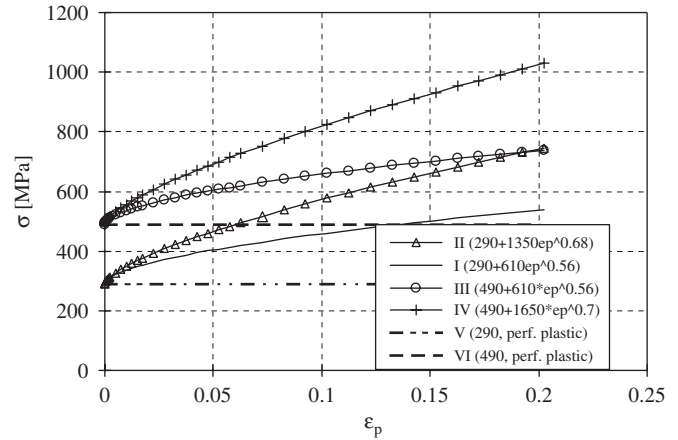


Fig. 5. Stress–plastic strain curves for selected parameters values.

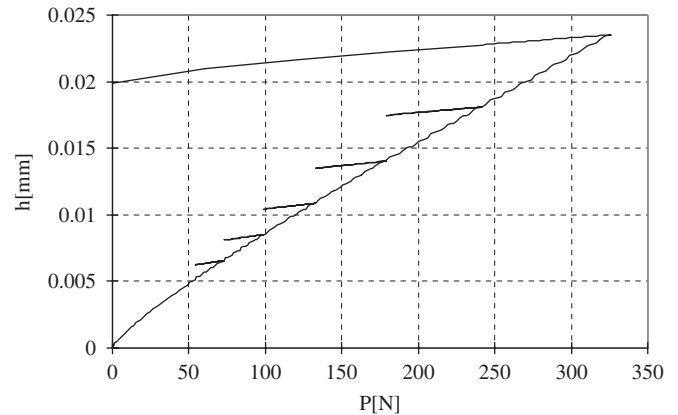


Fig. 6. Loading–partial unloading–reloading curve for material II determined numerically for sphere diameter $D = 2.5$ mm.

The identification procedure starts from determination of the loading–partial unloading–reloading curve in the spherical indentation test. For materials shown in Table 1, the penetration curves were determined by means of the finite element simulation. One of these curves, calculated for material II in the range of 0–326 N for load reversals at 73, 98, 133, 179, 242, and 326 N, is presented in Fig. 6.

Next, the points of the plastic compliance $h'_p(P)$ and plastic penetration $h_p(P)$ curves are specified (at values of P corresponding to load reversals) by subtracting at these points compliances of loading and unloading curves [19], and then the integration. However, the curves $h'_p(P)$, $h_p(P)$ so generated, differ from those specified by the postulated P – h_p relation (25), Fig. 2, corresponding to a rigid–plastic material (20). The difference is significant in the initial stage of indentation when only elastic strains occur and the plastic strains develop at a finite value of indentation force and finite contact area. On the other hand, for a rigid–plastic model, the plastic deformation develops in the initial stage of indentation. The penetration depth attained before the onset of plastic strain in the elastic–plastic material depends on the ratio E/σ_o . The difference between the responses of elastic–plastic and rigid–plastic

models diminishes with the growth of the ratio E/σ_o , when the elastic–plastic material tends to become rigid–plastic and for increasing penetration depths when the average elastic strains are much smaller than the plastic strains. Similarly, the function $c^2 = c^2(P)$ shown in Fig. 3 is

generated by the function $h_p = h_p(P)$ and for $P \rightarrow 0$ this function cannot be accurately specified.

Figs. 7–9 present the specified loading, unloading, and plastic compliances as functions of the indentation force P . The plastic parameters σ_o, k, m are selected from Table 1 and the specification procedure was carried out for different values of the ratios $s = E/\sigma_o$. For materials I and II, it was assumed that $s = E/\sigma_o = 345$ and $s = 410$, 345 and 260 for materials III and IV.

It can be noted that the plastic compliance moduli decrease monotonically for increasing value of P ; however, for small values of P there is a local maximum reached by the moduli. This maximum results from the fact that plastic deformation develops starting from a finite value of P . The character and position of the so-determined maximal plastic compliance depends on the value of $s = E/\sigma_o$. For instance, for materials III and IV and $s = 260$, the maximum of C^p occurs for larger values of P , Fig. 8b, than that for $s = 410$, Fig. 8a, or for $s = 520$, Fig. 9. From the diagrams in Figs. 7–9 it can be observed that the maximum value of plastic compliance calculated by means of subtraction method depends on E/σ_o and plastic

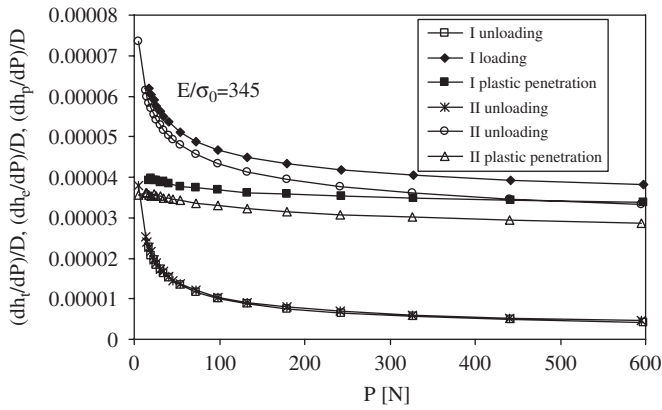


Fig. 7. Elastic–plastic, elastic and plastic compliance curves for materials I and II.

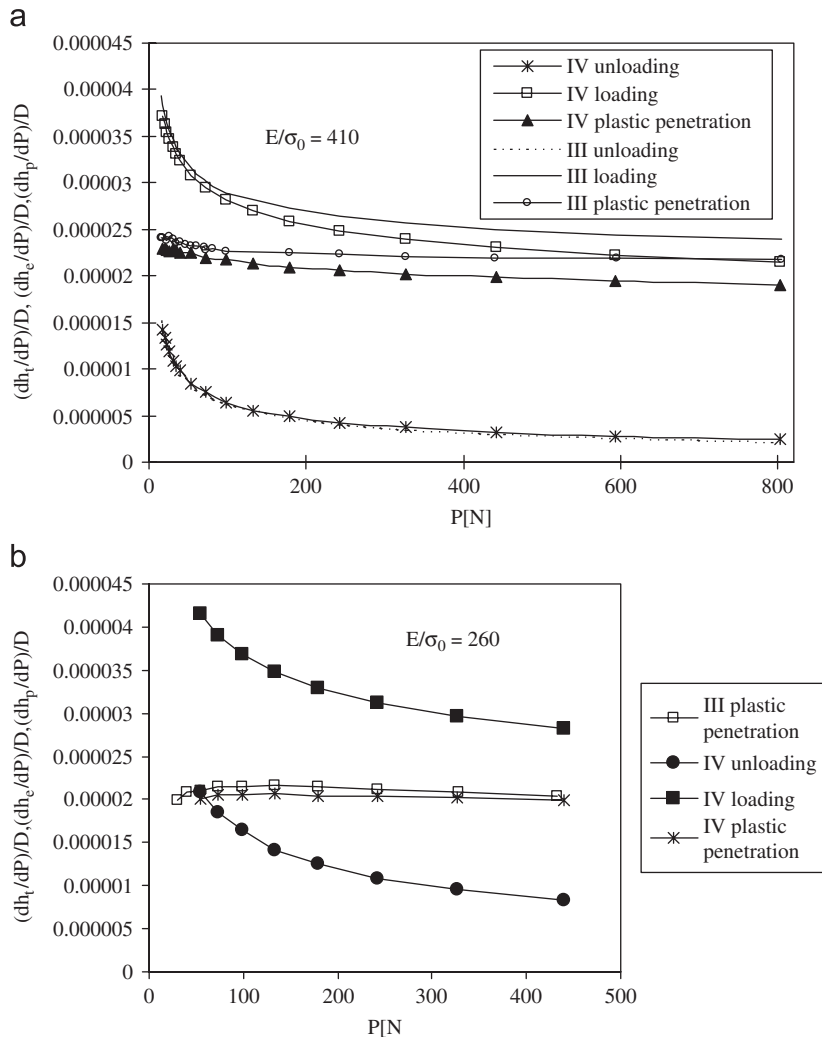


Fig. 8. Elastic–plastic, elastic and plastic compliance curves for materials III and IV: (a) for high ratio E/σ_o , (b) for low ratio of E/σ_o .

parameters k, m . Let us note that for $s = E/\sigma_o \rightarrow \infty$, the rigid–plastic response of contact occurs with the maximum compliance modulus reached at $P = 0$, Figs. 1b, 2.

For the identification procedure, the compliance curves are analytically extended to $P = 0$, thus neglecting the response for small values of P before reaching the maximal plastic compliance modulus. Fig. 10 presents the approximated compliance evolution of $C^p(P)$ for materials I–VI. The approximated compliance curves decrease monotonically in the whole range of loading and reach maximal values for $P = 0$.

Noting that for a rigid–plastic material

$$C^p(0) = \frac{1}{T} = \frac{1}{\pi\alpha D^2 c^2(0)\sigma_o}, \quad (33)$$

the yield strength value could be identified from Eq. (33). Practically, for actual materials which are elastic–plastic, it is assumed that the value of $C^p(0)$ is specified for very low value of P , denoted as P_{offs} (of order of 1 N in the case of materials described in the Table 1, for the assumed value of $D = 2.5$ mm), cf. Table 2. Generally, this offset value corresponds to the relative penetration depth h_p/D denoted as h_{offs}/D which is close to 4.7×10^{-5} for all considered

materials, cf. Table 2. For such defined values of P , the function C^p has the same values for materials I, II, V and III, IV, VI, respectively. It confirms our initial assumption that $T = 1/C^p(0)$ in Eq. (28) depends on σ_o and does not depend on hardening parameters k, m .

Fig. 11 presents the approximation procedure. To specify the remaining parameters, the proper curve portion should be used, namely after reaching the maximum modulus value. In fact, for larger penetration values, the compliance curve does not depend on the value of $s = E/\sigma_o$ and is close to a response predicted by the rigid–plastic model.

The results presented in Figs. 7–10 are recapitulated in Fig. 11. Two values of loading force are marked: the value P_y corresponds to the initiation of the plastic deformation of the indented material (at the Belyayev point) and P_M corresponds to a local maximum M of $C^p(P)$ observed in Figs. 7–9. If $E/\sigma_o \rightarrow \infty$ then $P_M \rightarrow 0$ and $P_y \rightarrow 0$. It should be noted that for actual materials the value of P_y is relatively small; for example, for $E/\sigma_o = 345$, (Fig. 9) there is $P_y = 0.4$ N. Obviously, the loads applied in the identification procedure should be greater than P_y . Moreover, to specify $C^p(P \approx 0)$, the proper portion of the generated $C^p(P)$ curve has to be used, i.e. it should start from a force P slightly greater than that corresponding to

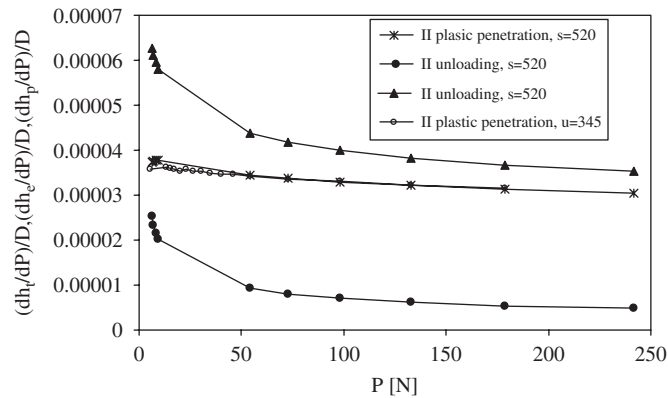


Fig. 9. Effect of E/σ_o ratio on the generated plastic compliance curve $C^p = C^p(P)$ for material II.

Table 2
Yield strength values identified for six materials

Number of $\sigma-\epsilon_p$ curve	h_{offs}/D	$1/T$	P_{offs}	σ_o (MPa)
I	4.70358E-05	4.49573E-05	1 N	286
II	4.76154E-05	4.59836E-05	0.95 N	281
III	4.69587E-05	2.62456E-05	1.7 N	450
IV	4.69635E-05	2.5391E-05	1.8 N	505
V	Whole range	4.373E-05	Whole range	295
VI	Whole range	2.5821E-05	Whole range	496

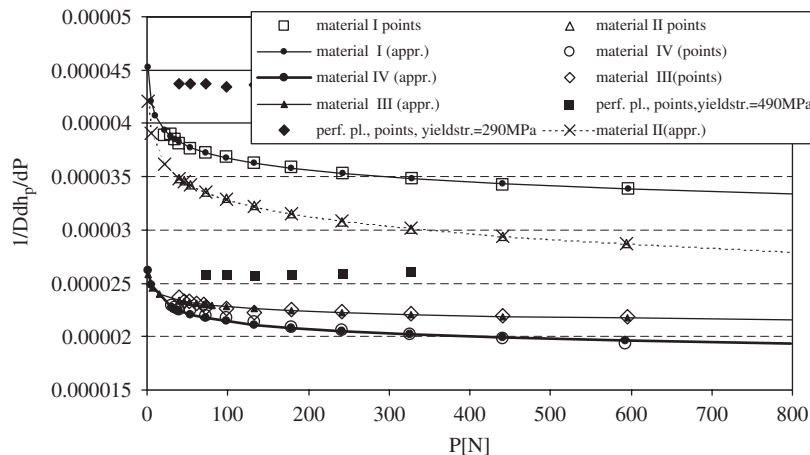


Fig. 10. Extrapolation of the generated plastic compliance curves, specification of $C^p(0)$ for $P \rightarrow 0$.

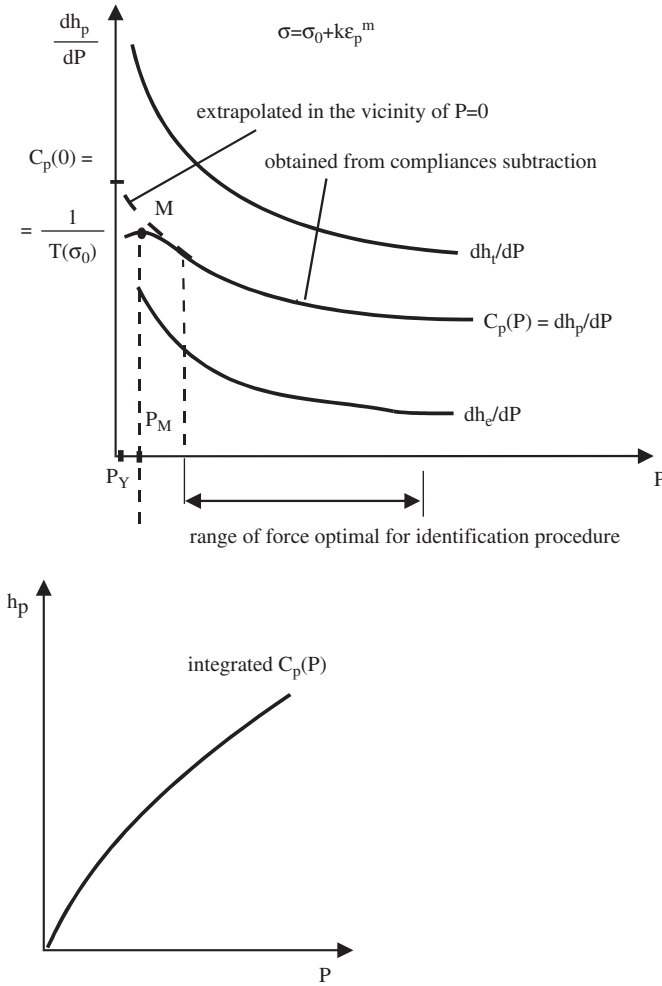


Fig. 11. The curves dh_p/dP , $h_p(P)$ generated by means of the proposed method for elastic-plastic material.

the local maximum M , and should not exceed the maximal force corresponding to the range of the similarity solution.

The identification procedure has to be reduced in the following special (limiting) cases: elastic-perfectly plastic and hardening Ramberg-Osgood materials. The elastic-perfectly plastic material is characterized by a constant value of the plastic compliance function $C^p(P)$, Fig. 1b, and thus it can be recognized (detected) at the first step of identification procedure. As the value of c^2 is also constant, $c^2 = 1.41$, the second step can be skipped and identification is terminated at step 3. The plastic compliance curve has the form of a horizontal line, Fig. 10, and its intersection with the ordinate axis is easy to determine. The parameter k in Eq. (28) should be assumed to vanish and this equation is now reduced to the first term, namely

$$Z_T \left(\frac{h_p}{D} \right) = T(\sigma_o) \frac{h_p}{D}. \tag{34}$$

The Ramberg-Osgood material, $\sigma = k\epsilon_p^m$, can be recognized at the second step of the identification procedure. For such material the value of c^2 is constant and less than 1.41. Eq. (28) is reduced to the second term. To identify the

parameters k and m , one should apply the procedure presented in our previous paper [19].

The results of identification for considered materials I–VI are shown in Table 2 and in Fig. 12. Table 2 presents the values of yield stress determined from Eq. (30) in the first three steps of the identification procedure.

Fig. 12 presents a comparison of the actual and identified curves for materials I–IV. The accuracy of the method can be estimated as satisfactory.

To illustrate the sensitivity of results obtained by means of the proposed method with respect to the small variation of the identified stress-strain curve, and to demonstrate the accuracy of the method in a case of simplified linear hardening stress-strain characteristic, an additional example was calculated. In this example, one has identified the linear hardening material (called as “CH” material) whose stress-strain curve is specified by the equation $\sigma = 300 + 1400\epsilon_p$ and presented in Fig. 13, where the $\sigma-\epsilon_p$ curve of the material I is also shown. It can be seen that these two materials (CH and I) are very similar; the CH material has the slightly greater yield stress but smaller hardening modulus in the initial stage of deformation than

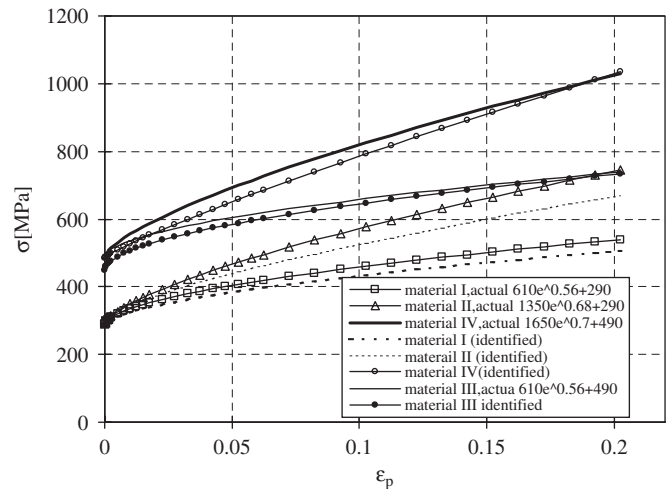


Fig. 12. Actual and identified stress strain curves.

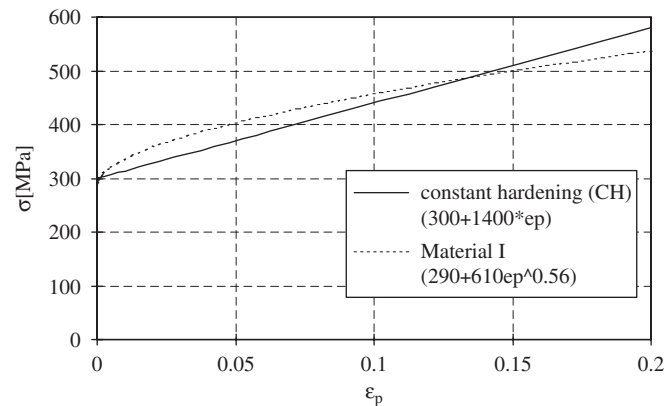


Fig. 13. Comparison of the plastic strain-stress curves of material I and a linearly hardening material.

material I. For larger values of strain, the slope of the CH material curve is lower than that of material I.

Fig. 14 shows points of the plastic compliance curves generated by means of the proposed method for the materials CH and I. For material CH, the analytical approximation curve is drawn and next extrapolated to identify the yield point.

From Figs. 12 and 13, it results that the shape of plastic compliance curves exactly corresponds to the material behavior described by means the of $\sigma-\varepsilon_p$ curves. For small strain range, the CH material is less stiff than material I and consequently in the indentation test for low loading values, the plastic compliance curve of material CH is located above the compliance curve of material I. For larger values of strain, material CH is stiffer than material I but the compliance curves of both materials coincide for higher loading values. This is due to the fact that for large loading, the penetration curve can be considered as the mean result of large deformations which appear in the vicinity of the contact area and lower deformations present at larger distances from the indenter tip. Thus, the penetration curve can be considered as a measure of the material stress–strain curve. The actual and identified stress strain curves for material CH are compared in Fig. 15.

4.1. Application of the proposed identification method: physical experiment

To demonstrate the accuracy of the proposed method, a physical example was also provided. The method was applied to identify the stress–strain curve of an aluminium alloy (commercial mark PA4). The cyclic loading–unloading–reloading indentation test was done by means of the spherical indenter ($D = 0.4\text{ mm}$). The penetration curve was measured in two ranges: 0–3 N, with load reversals at 0.5, 1, 1.6, 2.4, 3, and 0–17.8 N with load reversals at 3, 4, 5.5, 7.5, 10, 13.5, 17.8 N. For the latter range, two measured penetration curves for two samples are compared in Fig. 16 to illustrate the scatter of results.

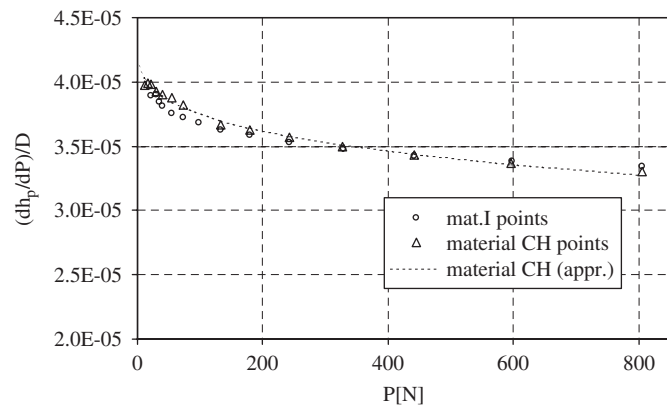


Fig. 14. Comparison of the plastic compliance curves of material I and a linearly hardening material.

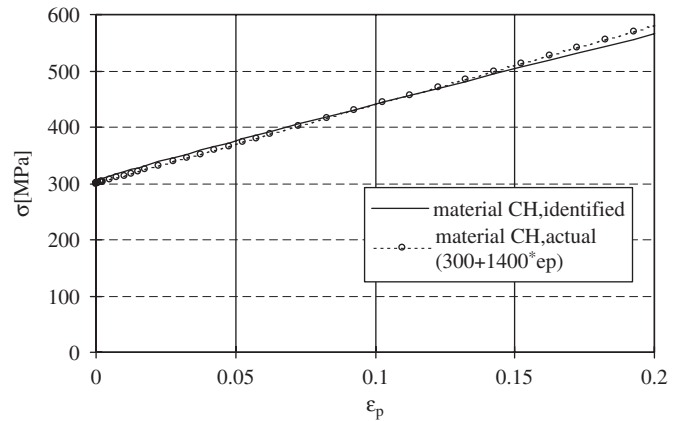


Fig. 15. Identified and actual stress–strain curves for material CH.

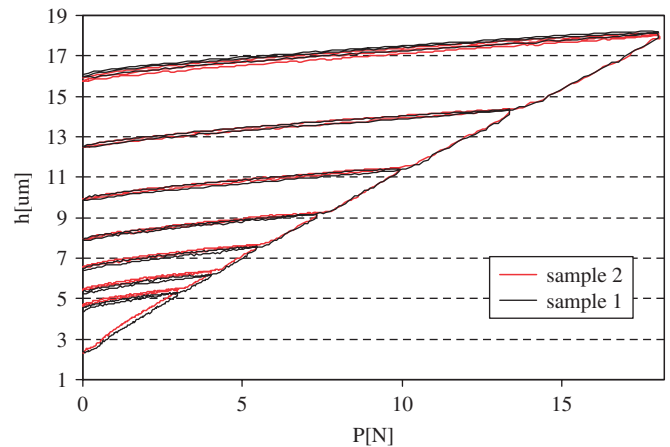


Fig. 16. Cyclic penetration curves for aluminium alloy (physical experiment).

The elastic–plastic penetration curves $h_i(P)$, Fig. 16, for loading and unloading were separately approximated with continuous functions by means of nonlinear curve fitting procedures. Next, the elastic and elastic–plastic compliances were calculated as derivatives of these functions at the load reversal points and the points of the plastic compliance curve were generated. The results are presented in Fig. 17.

The diameters ($2a$) of residual indentation imprints for large loads were measured by means of optical microscopy, and for small loads by means of scanning profilometry. The specified values were used to calculate the variation of $c_a^2(P_i)$. Next the proposed formulae were applied to determine the initial yield stress and the hardening curve. The result is presented in Fig. 18 where the identified stress–plastic strain curve is compared with the actual curve obtained in tension test.

It can be observed that the difference between the two curves in Fig. 18 reaches about 10%. The accuracy of identification is lower as compared to the case of numerical experiments. The error results from the difficulties in exact measurement of contact radius a , particularly in the low range of loading. The inaccuracy occurs also due to higher

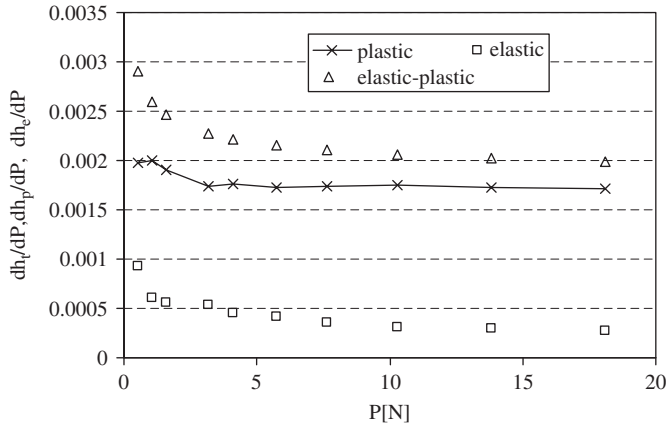


Fig. 17. Elastic-plastic, elastic and plastic compliance curves for aluminium alloy.

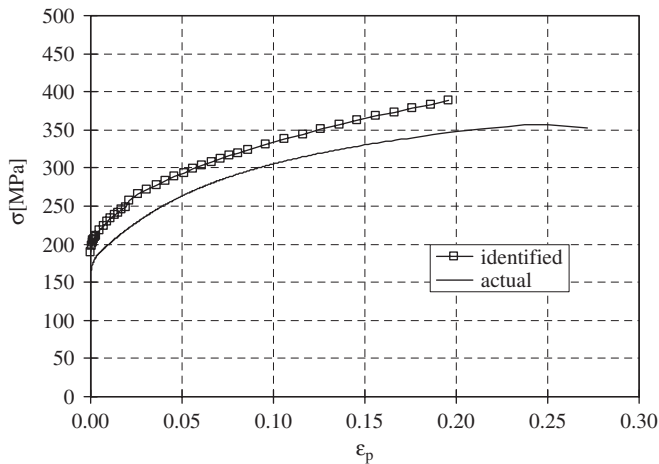


Fig. 18. Tension curves for aluminium alloy: identified by means of the proposed method and obtained in tension test.

noise to signal ratio in the measurement apparatus in the low range of loading, which is manifested by a non-monotonic character of the specified plastic compliance curve. It should be noted that the identified curve is stiffer than the actual one. This effect can result from surface hardening due to the grinding and polishing process before indentation testing. However, the obtained accuracy seems to be acceptable.

5. Conclusions

This paper presents a new procedure for determining the plastic stress–strain curve by means of a cyclic spherical indentation test. Three model parameters occurring in the Ludwig law $\sigma = \sigma_0 + k\epsilon_p^m$ were identified. Starting from the general solution of the spherical indentation test presented in the paper by Hill et al. [1], we proposed a new approximate formulae which correlates an elastic–plastic penetration curve, its derivatives, and radius of contact boundary, with three parameters of the constitutive model. In view of these formulae, the special identification

procedure was developed. To apply the procedure, one should measure the cyclic loading–unloading–reloading penetration curve and the radius of contact boundary at the points of loading reversals. Taking into account previous works of the authors, it can be concluded that the identification of two material parameters (Ramberg–Osgood model) requires a measurement of two quantities: force and penetration depth. However, to identify three parameters (Ludwig model), one should measure three quantities: force, penetration depth, and contact radius. Similar conclusions result from the work [15], where both indentation depth and contact area also have to be measured in a sharp indentation test. It should be noted that most identification methods reviewed in Section 1 are concerned with identification of two plastic hardening parameters of the stress–strain curve.

To verify the procedure, the parameters of seven materials were identified. The required indentation parameters were specified using numerical indentation experiments. The accuracy of the results is satisfactory, however it can be improved by better evaluation of the constants β_1 and w in Eqs. (28) and (29). A more accurate evaluation can be achieved by means of extensive numerical simulations for various combinations of material properties. The accuracy of the method depends also on the curve fitting procedure applied to approximate the points of elastic–plastic penetration curve which have to be differentiated, thus generating the plastic compliance curve, dh_p/dP , which is used to specify σ_0 and then is integrated to obtain $h_p(P)$. The curve fitting process should be executed very carefully. From the sequence of steps in the identification procedure, it follows that the error in identification of the initial yield stress affects the accuracy of parameters k and m specified in the next step. However, one can observe in the case of material III, that even if the error of σ_0 is relatively significant, the determined hardening moduli are greater in the small strain range than the actual values, and the whole plastic hardening curve is determined with good accuracy, Fig. 12.

It should be noted that the accuracy of the proposed method is considerably better in the case of numerical experiments than in the case of presented physical experiment. This fact can result from errors in the determination of compliances (derivatives) of experimentally specified penetration curves and in the measurement of a .

The accuracy of the physical example can be considerably improved using a more accurate experimental stand. The method is very sensitive to the accuracy of the contact radius measurement.

The proposed procedure together with the method of Young modulus identification presented in Ref. [19] allows for specification of four parameters of the elasto-plastic tension curve from the spherical indentation test. This constitutes an essential improvement with respect to available methods. However, further work leading to refinement of the procedure is required.

Acknowledgements

This paper was partially supported by the grant No. 3T08C 02129 of Ministry of Science and Higher Education.

References

- [1] Hill R, Storakers B, Zdunek AB. A theoretical study of the Brinell hardness test. *Proceedings of the Royal Society of London* 1989;423:301–30.
- [2] Biwa S, Storakers B. An analysis of fully plastic Brinell indentation. *Journal of Mechanics and Physics of Solids* 1995;43:1303–33.
- [3] Field JS, Swain MV. Determining the mechanical properties of small volumes of material from submicrometer spherical indentations. *Journal of Materials Research* 1995;10(1):101–12.
- [4] Adler TA, Dogan ON. Damage by indentation and single impact of hard particles on a high chromium white cast iron. *Wear* 1997;203–204:257–66.
- [5] Taljat B, Zacharia T, Kosel F. New analytical procedure to determine stress–strain curve from spherical indentation data. *International Journal of Solids and Structures* 1998;35:4411–26.
- [6] Kucharski S, Mróz Z. Identification of plastic hardening parameters of metals from spherical indentation tests. *Materials Science & Engineering A* 2001;318(1–2):65–76.
- [7] Kucharski S, Mróz Z. Identification of hardening parameters of metals from spherical indentation test. *Journal of Engineering Materials and Technology—Transactions of the ASME* 2001;123:245–50.
- [8] Huber N, Tsakmakis Ch. A finite element analysis of the effect of hardening rules on the indentation test. *Journal of Engineering Materials and Technology—Transactions of the ASME* 1998;120:143–8.
- [9] Huber N, Tsakmakis Ch. Determination of constitutive properties from spherical indentation data using neural networks. Part I: the case of pre kinematic hardening in plasticity laws. *Journal of Mechanics and Physics of Solids* 1999;47:1569–88.
- [10] Huber N, Tsagrakis I, Tsakmakis Ch. Determination of constitutive properties of thin metallic films on substrates by spherical indentation using neural networks. *International Journal of Solids and Structures* 2000;37:6499–516.
- [11] Mesarovic SDJ, Fleck NA. Spherical indentation of elastic–plastic solids. *Proceedings of the Royal Society of London Series A* 1999;455:2707–28.
- [12] Nayebi A, El Abdi R, Bartier O, Mauvoisin G. New procedure to determine steel mechanical parameters from the spherical indentation technique. *Mechanics of Materials* 2002;34:243–54.
- [13] Nayebi A, Bartier O, Mauvoisin G, El Abdi R. New method to determine the mechanical properties of heat treated steels. *International Journal of Mechanical Science* 2001;43:2679–97.
- [14] Giannakopoulos AE, Suresh S. Determination of elastoplastic properties by instrumentated sharp indentation. *Scripta Materialia* 1999;40:1191–8.
- [15] Tunvisut K, Busso EP, O’Dowd NP. Determination of the mechanical properties of metallic thin films and substrates from indentation tests. *Philosophical Magazine A* 2002;82(10):2013–29.
- [16] Johnson KL. The correlation of indentation experiments. *Journal of Mechanics and Physics of Solids* 1970;18:115–26.
- [17] Gao X-L, Jing XN, Subhash G. Two new expanding cavity models for indentation deformations of elastic strain-hardening materials. *International Journal of Solids and Structures* 2006;43:2193–208.
- [18] Cao YP, Lu J. A new method to extract the elastic properties of metal materials from an instrumented spherical indentation loading curve. *Acta Materialia* 2004;52:4023–32.
- [19] Kucharski S, Mróz Z. Identification of material parameters by means of compliance moduli in spherical indentation test. *Materials Science & Engineering A* 2004;379:448–56.
- [20] Park YJ, Pharr GM. Nanoindentation with spherical indenters: finite element studies of deformation in the elastic–plastic transition regime. *Thin Solid Films* 2004;447–448:246–50.